WELDING RESEARCH

SUPPLEMENT TO THE *WELDING JOURNAL*, APRIL 2006
Sponsored by the American Welding Society and the Welding Research Council

Microstructure and Microchemistry of Hard Zone in Dissimilar Weldments of Cr-Mo Steels

Different types of carbides and their quantities are identified in weldments between 9Cr-1Mo and 2¼Cr-1Mo ferritic steel that was postweld heat treated

BY C. SUDHA, V. THOMAS PAUL, A. L. E. TERRANCE, S. SAROJA, AND M. VIJAYALAKSHMI

ABSTRACT. This paper reports the microstructure and microchemistry of "hard" and "soft" zones in a dissimilar weldment between 9Cr-1Mo and 2¼Cr-1Mo ferritic steel subjected to postweld heat treatments (PWHT). Diffusion of carbon driven by the activity gradient across the weld interface is found to result in the formation of a soft zone in the low-Cr side and a carbide-rich hard zone adjoining the soft zone in the high-Cr side of the weldment. Detailed analytical transmission electron microscopy (ATEM) studies were essential to evaluate a number of microstructural parameters based on which the variation of concentration of carbon across the hard zone was derived using mass balance equation. The concentration of carbon in the hard zone thus arrived follows the same trend as that of the variation of area fraction of carbides with distance across the hard zone.

Introduction

Weldments joining different kinds of heat-resistant steels are used for high-temperature applications in fossil-fueled power plants, and the chemical, petrochemical, and nuclear industries. Dissimilar weldments, especially between low-Cr and high-Cr ferritic steel, are used in a number of steam generator circuits. It is well known that carbon migration occurs across the weld interface from low-alloy ferritic steel to high-alloy ferritic steel during exposure to high temperature. This results in the formation of a carbon-denuded soft zone characterized by low hardness in the low-alloy side and a carbon-enriched hard zone on the high-alloy side of the weld interface. Studies on the formation of soft and hard zones in dissimilar weldments during PWHT are essential for the prediction of microstructural instability during prolonged exposure at the operating temperature. These microstructural instabilities would lead to severe degradation in the mechanical properties of the weldments.

Several investigations (Refs. 1–4) have been made to study the microstructural changes introduced near the weld interface due to the migration of carbon. These studies showed that on subjecting the weldments to PWHT, carbon migration dictated by the carbon activity gradient occurs leading to the formation of a soft zone in the low-Cr steel with an adjoining precipitate-rich hard zone in high-Cr steel.

Carbon activity diagrams were proposed (Ref. 1) to aid the selection of welding consumables that would prevent the formation of these hard brittle zones. It was shown (Refs. 5, 6) that these zones are susceptible to failure when subjected to creep and tensile tests. Room-temperature tensile tests showed that even though deformation started at the soft zone, the constricting effect of the hard zone and the strain hardening of the soft zone shifted the site of maximum stress to the 2¼ Cr base metal side. But fracture occurred at the soft zone during high-temperature stress rupture tests. Creep tests (Ref. 7) done in a dissimilar weldment between 1CrMoV and 12CrMoV using filler metals with 5 and 12% Cr showed fracture initiation in the soft zone. Analysis for the distribution of carbon across the interface of dissimilar weldments was done and theoretical equations were proposed (Refs. 8–10) to calculate the width of carburized and decarburized zones. Though the carbide-rich hard zone is almost always associated with carbon redistribution, direct experimental evidence for weldments of Cr-Mo ferritic steels does not exist. An attempt (Ref. 2) was made earlier to determine the elemental redistribution (mainly of Cr, Mo) across the weld interface, and based on the microchemistry to identify the nature of carbides in hard and soft zones in dissimilar weldments between 9Cr-1Mo and 2¼Cr-1Mo ferritic steel. The estimation of a carbon profile has not been attempted so far. The type of carbides and evolution of carbides for different PWHT parameters has not been studied. Hence, a detailed investigation has been carried out to obtain direct confirmatory evidence for the enrichment of carbon in the hard zone and to establish the sequence of precipitation of carbides.

This paper gives a detailed study of hard and soft zones in dissimilar weldments between 9Cr-1Mo and 2¼Cr-1Mo ferritic steels subjected to PWHT of 750°C (1023 K) for 1–15 h. Evolution of different types of carbides, their type, amount, and microchemistry in the hard zone, has been investigated using analytical transmission electron microscopy (ATEM). Based on these experimental data, carbon redistribution across the

C. SUDHA, V. THOMAS PAUL, A. L. E. TERRANCE, S. SAROJA, and M. VIJAYALAKSHMI (mvl@igcar.ernet.in) *are with Physical Metallurgy Section, Materials Characterization Group, Indira Gandhi Center for Atomic Research, Kalpakkam, India.*

KEYWORDS

Ferritic Steels
Dissimilar Weldments
Diffusion
Carbides
Analytical Transmission
Electron Microscopy

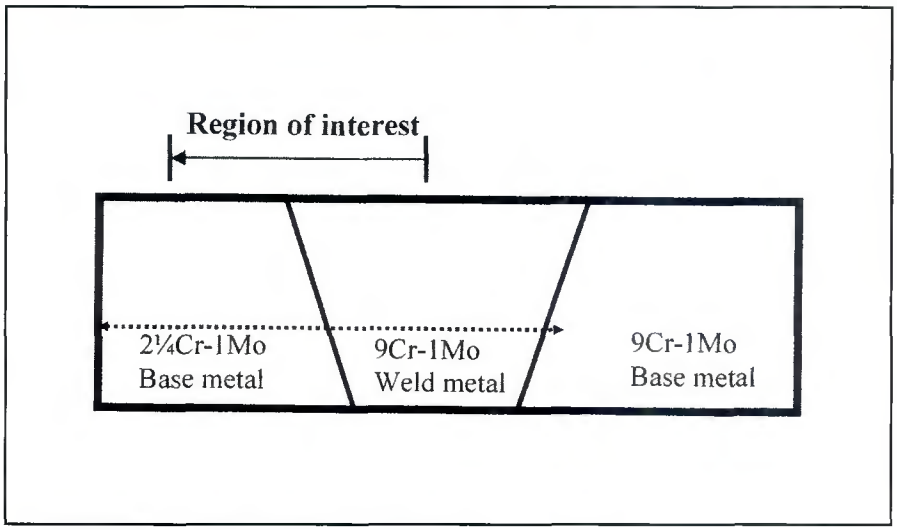

Fig. 1 — Cross section of the weldment under study (dotted lines indicate the plane of observation and continuous line shows the region of interest).

Table 1 — Chemical Composition of the Steel Plates and the Weld Metal

Sl. No.	Description	Element (wt-%)						
		C	Cr	Mo	Mn	S	P	Si
1	2¼Cr-1Mo Plate	0.12	2.18	1.0	0.46	0.001	0.01	0.25
2	9Cr-1Mo Plate	0.07	8.24	1.0	0.36	0.001	0.02	0.21
3	9Cr-1Mo Weld Metal (Electrode)	0.08	10.25	0.98	0.91	0.02	0.02	0.40

Table 2 — Welding Parameters Employed for Preparation of Weld Pads

Electrode dia. (mm)	Preheat Temp. (K)	Current (A)	Voltage (V)	Welding Speed (mm/min)	Joint Geometry	Bead Tech	No. of passes
4	493	160–175	26	140	Single-V Root opening 2 mm Included angle 110 deg	Stringer	8

hard zone has been evaluated, thus providing for the first time direct confirmation for the origin of the hard zone.

Experimental Details

Weldments of 9Cr-1Mo and 2¼Cr-1Mo steel were prepared using plates of 12.5-mm thickness supplied in normalized and tempered conditions. The nominal composition of the steels is given in Table 1. Shielded metal arc welding (SMAW) was employed in the preparation of a single-V groove weld using 9Cr-1Mo as the electrode. The welding parameters are given in Table 2. Postweld heat treatment was given at a temperature of 1023 K for durations ranging from 1 to 15 h. The specimens were prepared by conventional metallographic procedures (polishing and etching using 2% Nital) for microstructural investigations. Nital being a mild reagent etches only the 2¼Cr-1Mo side. Microstructural examination was carried out using a Leica MEF4A optical microscope. Scanning electron microscopy was carried out using a Philips XL30 ESEM at an operating voltage of 10–20 keV. Cameca SX 50 electron probe micro analyzer (EPMA) at an operating voltage of 20 keV was used to investigate chromium redistribution across the weld interface. The cross section of the weldment on which the analytical transmission electron microscopy (ATEM) study was carried out is shown in Fig. 1. The region of interest in the present study is confined to the interface between the 2¼Cr-1Mo base metal and 9Cr-1Mo weld metal and the plane of observation is along the middle section of the weld as shown by dotted lines in Fig. 1.

Carbon extraction replicas a few micrometers thick were selected from the hard zone and prepared as follows:

After etching the sample with 2% Nital solution, the hard zone alone was carbon coated by masking the remaining regions of the sample with aluminum foil. After carbon coating, the aluminum foil was removed, leaving a thin film of carbon along the hard zone of the sample. On etching the sample again with 2% Nital solution, the carbon film with the extracted carbides could be removed from the surface of the sample. These films were collected on a 200-mesh grid for ATEM analysis. Detailed microstructural and microchemical investigations were carried out on carbon extraction replicas using a Philips CM 200 analytical electron microscope with EDAX, DX4 analyzer and a super ultra-thin window.

Selected area diffraction (SAD) patterns obtained from the carbides were analyzed to identify the type of carbides. The EDAX spectra obtained from various carbides were also characteristic of the carbide. It was used for identification of the type of carbide and also for quantification of the composition using Fe Kα, Cr Kα, and Mo Lα lines. Around ten spectra were obtained from each type of carbide. Quantification of the spectra required evaluation of Cliff Lorimer constants (i.e., k_{AB} values). A sample of 316 stainless steel of known chemical composition was used for the purpose of evaluating k_{AB} values, under identical experimental conditions. These k_{AB} values were used for the quantification of EDAX spectra using the following Cliff Lorimer equation:

$$\frac{C_A}{C_B} = k_{AB}\frac{I_A}{I_B} \qquad (1)$$

where C_A and C_B refer to the concentration of A and B in alloy AB. I_A and I_B are the X-ray intensities for A and B.

The concentration of all the elements in the carbides thus evaluated was found to agree with those obtained by wet chemical analysis of the carbide extracted by chemical dissolution methods (Ref. 11). The carbon present in the α-ferrite could not be determined due to its low concentration. An indirect method adopted to arrive at the carbon concentration in carbides is described in Appendix 1.

In order to identify the different types of carbides and their area fraction (A_p) as a function of distance from the interface, the hard zone was assumed to be divided into 30 rectangular areas or slabs of equal size parallel to the interface. The area fraction of each type of carbide in each slab was determined graphically. Then the total area fraction of carbides in each slab

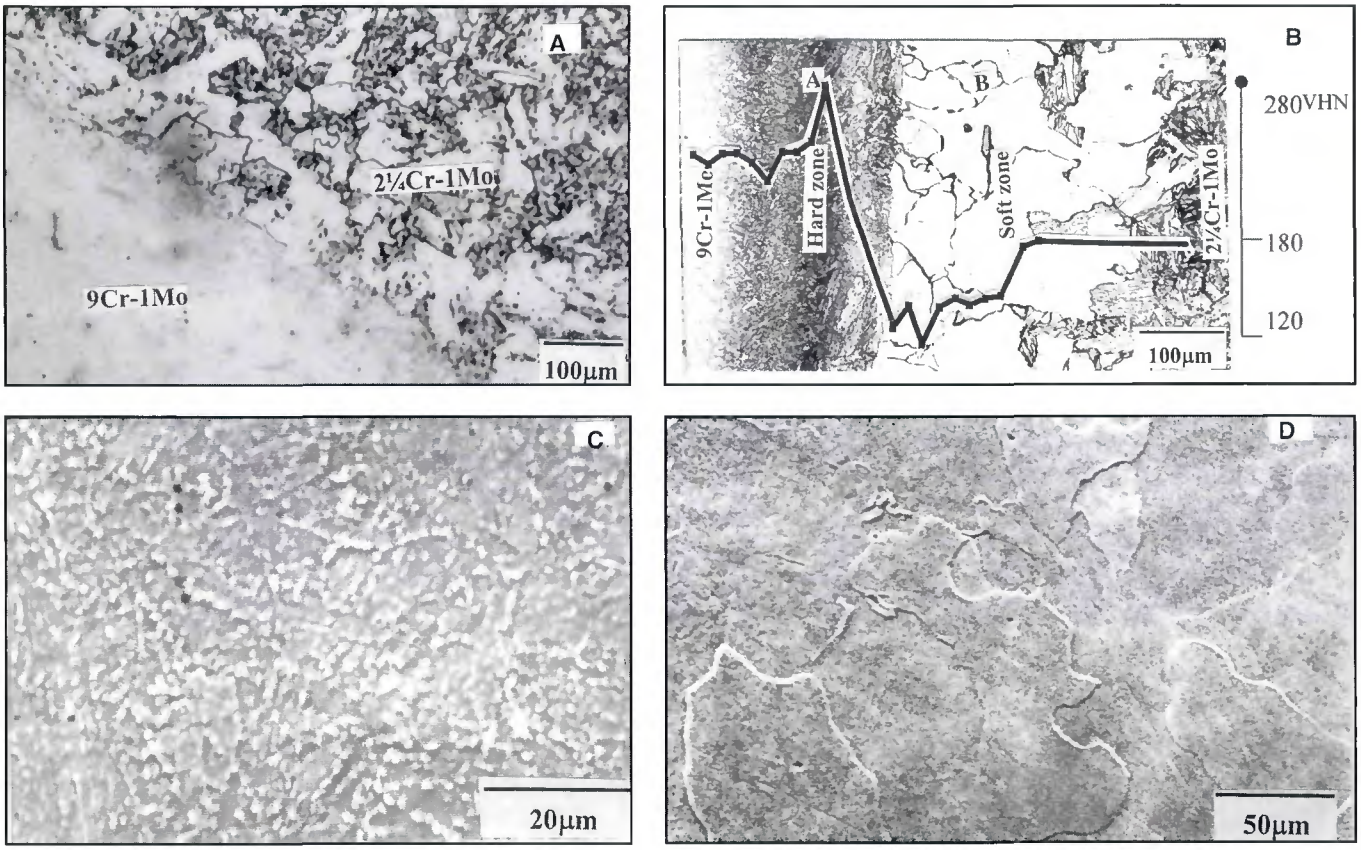

Fig. 2 — Optical micrographs. A — As-welded structure; B — formation of hard and soft zones (hardness profile superimposed) in a sample exposed for 15 h at 1023 K and etched with 2% Nital; C — SE image of precipitates in hard zone; D — SE image of ferrite grains in soft zone, devoid of secondary phases.

Table 3 — Types of Carbides Identified and the Distribution of Major Alloying Elements in Them

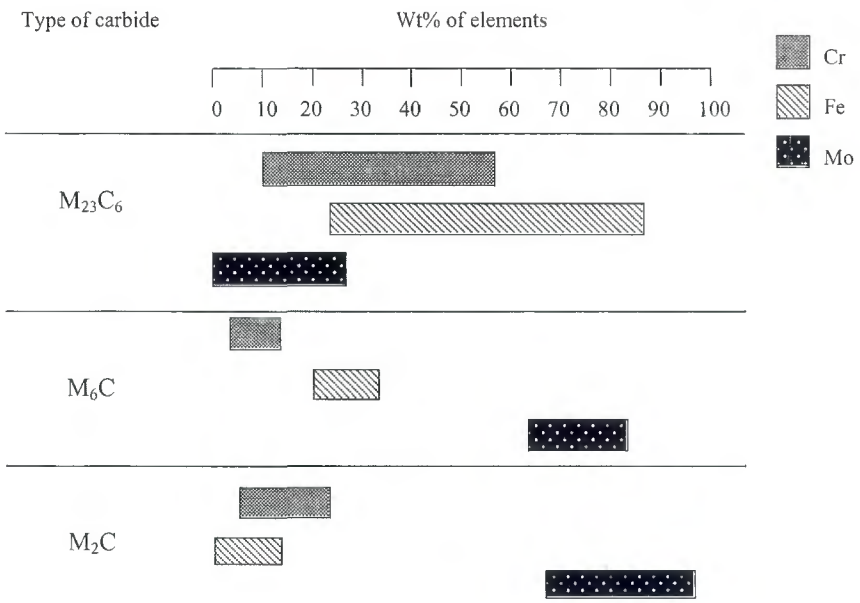

was calculated as

$$A_p = A_A + A_B \qquad (2)$$

where A_p = total area fraction of carbides in a slab, and $A_A + A_B$ = area fraction of carbides of types A and B.

The values thus calculated from several slabs were found to be accurate to only within ±10%. The sources of error in this calculation are a) statistical scatter, b) assumption that the distribution of carbides in the carbon extraction replica is a true representation of the same in the sample, and c) nonuniform distribution of carbides. However, these sources of inaccuracy have been found to be insignificant due to the following advantages:

1) A carbon extraction replica represents the distribution of carbides over a larger number of grains than thin foil and, therefore, provides a better statistical representation of the distribution of carbides.

2) Examination of many replicas for the same treatment revealed no significant differences in the distribution of carbides.

3) Similar procedure adopted in the case of 9Cr-1Mo steel (Ref. 11) revealed

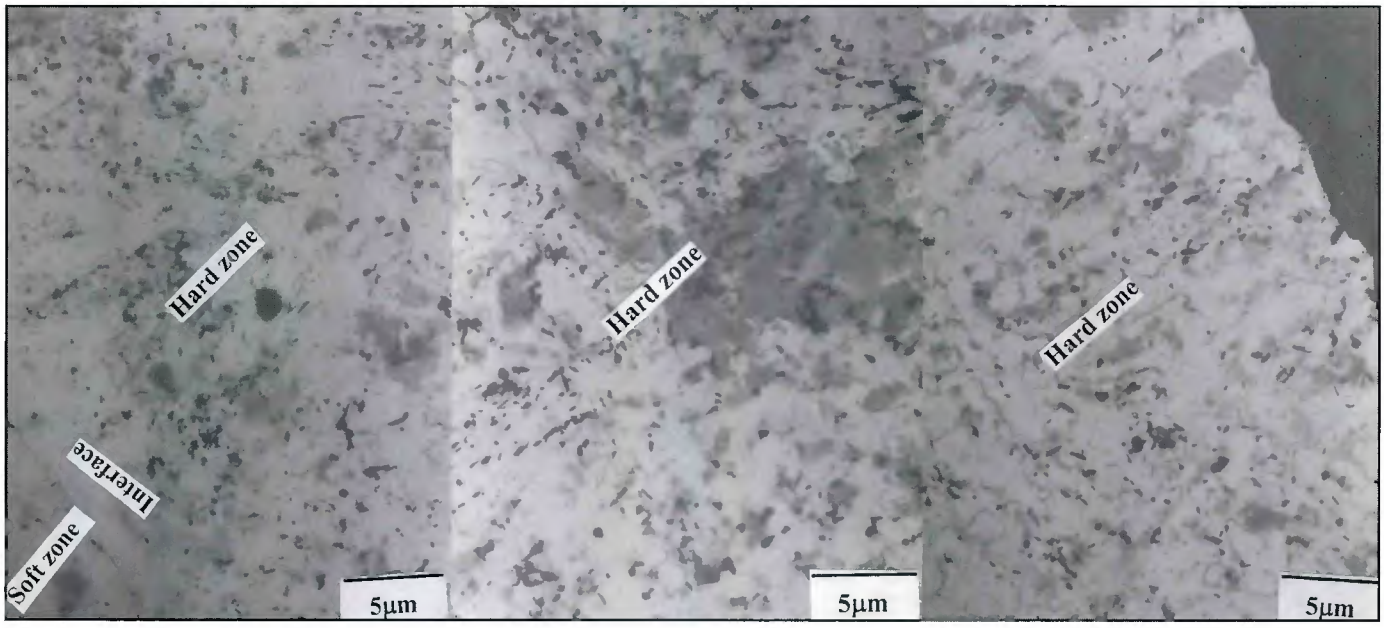

Fig. 3 — Low-magnification TEM micrographs showing distribution of precipitates in hard zone.

Table 4 — Details of Analysis of Types of Carbides and their Chemistry

Tempering Time (h)	Precipitate Type	at.-% M in Metal Sub Lattice at.-% Σ = ± 10%			Stoichiometry of the Carbides
		Fe	Cr	Mo	
1	$M_{23}C_6$	57.0	32.7	11.7	$Fe_{13.1}Cr_{7.5}Mo_{2.7}C_6$
		75.2	20.3	4.5	$Fe_{17.3}Cr_{4.7}MoC_6$
		39.2	53.1	7.8	$Fe_9Cr_{12.2}Mo_{1.8}C_6$
	M_2C	2.1	12.9	85.0	$Fe_{0.1}Cr_{0.3}Mo_{1.7}C$
2	$M_{23}C_6$	54.9	31.0	11.7	$Fe_{12.6}Cr_{7.1}Mo_{2.7}C_6$
		77.8	20.9	1.3	$Fe_{17.9}Cr_{4.8}Mo_{0.3}C_6$
		40.0	51.7	8.4	$Fe_{9.2}Cr_{11.9}Mo_{1.9}C_6$
	M_2C	2.4	21.5	76.2	$Fe_{0.1}Cr_{0.4}Mo_{1.5}C$
5	$M_{23}C_6$	31.3	59.4	2.1	$Fe_{7.2}Cr_{13.7}Mo_{2.1}C_6$
		52.2	46.2	1.7	$Fe_{12}Cr_{10.6}Mo_{0.4}C_6$
		80.7	18.8	0.5	$Fe_{18.6}Cr_{4.3}Mo_{0.1}C_6$
15	$M_{23}C_6$	32.4	55.2	12.4	$Fe_{7.5}Cr_{12.7}Mo_{2.9}C_6$
		52.3	34.5	3.1	$Fe_{12}Cr_{7.9}Mo_{3.1}C_6$
	M_6C	28.0	4.9	67.2	$Fe_2Cr_{0.3}Mo_{3.7}C$

that measured values of A_p are in agreement with those obtained from the weight fraction of precipitates by the chemical extraction procedure.

Since this procedure has been verified for 9Cr-1Mo steel, it is reasonable to extend it to the case of weldments.

After determining the area fraction and type of carbides in each slab, the total amount of carbon in each slab in the hard zone was evaluated from the mass balance equation

$$C_0 = C_\alpha A_\alpha + \Sigma_p C_p A_p \qquad (3)$$

where C_0 = total amount of carbon in each slab; C_α = amount of carbon present in α-ferrite (value taken as 0.002, which is the maximum solubility limit of carbon in α-ferrite for an alloy with about 9% Cr); C_p = amount of carbon in carbides (p – $M_{23}C_6$, M_6C, etc.); A_p = area fraction of the precipitates; A_α = area fraction of ferrite (i.e., 1-A_p).

Results

The optical microstructure of the weldment in an as-welded condition is shown in Fig. 2A. The 9Cr side has not been etched by the reagent while the 2¼Cr side shows a predominantly tempered bainitic structure. Figure 2B shows the optical microstructure of the weldment subjected to a PWHT at 1023 K for 15 h. Microstructural changes are observed in regions close to the interface in the weld as well as in the base metal side. Superposition of the measured microhardness profile on the micrograph in Fig. 2B shows that the heavily etched region marked A has a high hardness (282 VHN) compared to the rest of the weldment. In contrast, the lightly etched region marked B in Fig. 2B, called the soft zone, is found to have a low hardness of only 124 VHN. The SEM micrographs in Fig. 2C and D showed that the hard zone is characterized by an uniform distribution of a high density of fine precipitates, while the soft zone is marked by the formation of large grains of α-ferrite due to dissolution of the preexisting cementite particles in bainite. On either side of the hard zone, the high density of fine precipitates typical of the hard zone was not observed.

The TEM micrograph in Fig. 3 shows the distribution of carbides from different regions of the hard zone. It was observed that on either side of the hard zone, the number density of carbides reduced significantly. Figure 4A and B shows the electron micrographs of carbides extracted from the hard zone of a weldment exposed to PWHT for 15 h. Various morphologies of carbides, either coarse globular, coarse lenticular, or fine needle shaped are observed. The insets in Fig. 4A and B show the SAD patterns from an acicular and globular precipitate of $M_{23}C_6$ along $< 2\,\bar{1}\,\bar{1} >$ and $< 3\,2\,\bar{1} >$, respectively. The EDAX spectra obtained from the two precipitates is shown in Fig. 4C and D. The precipitates were found to be either rich in

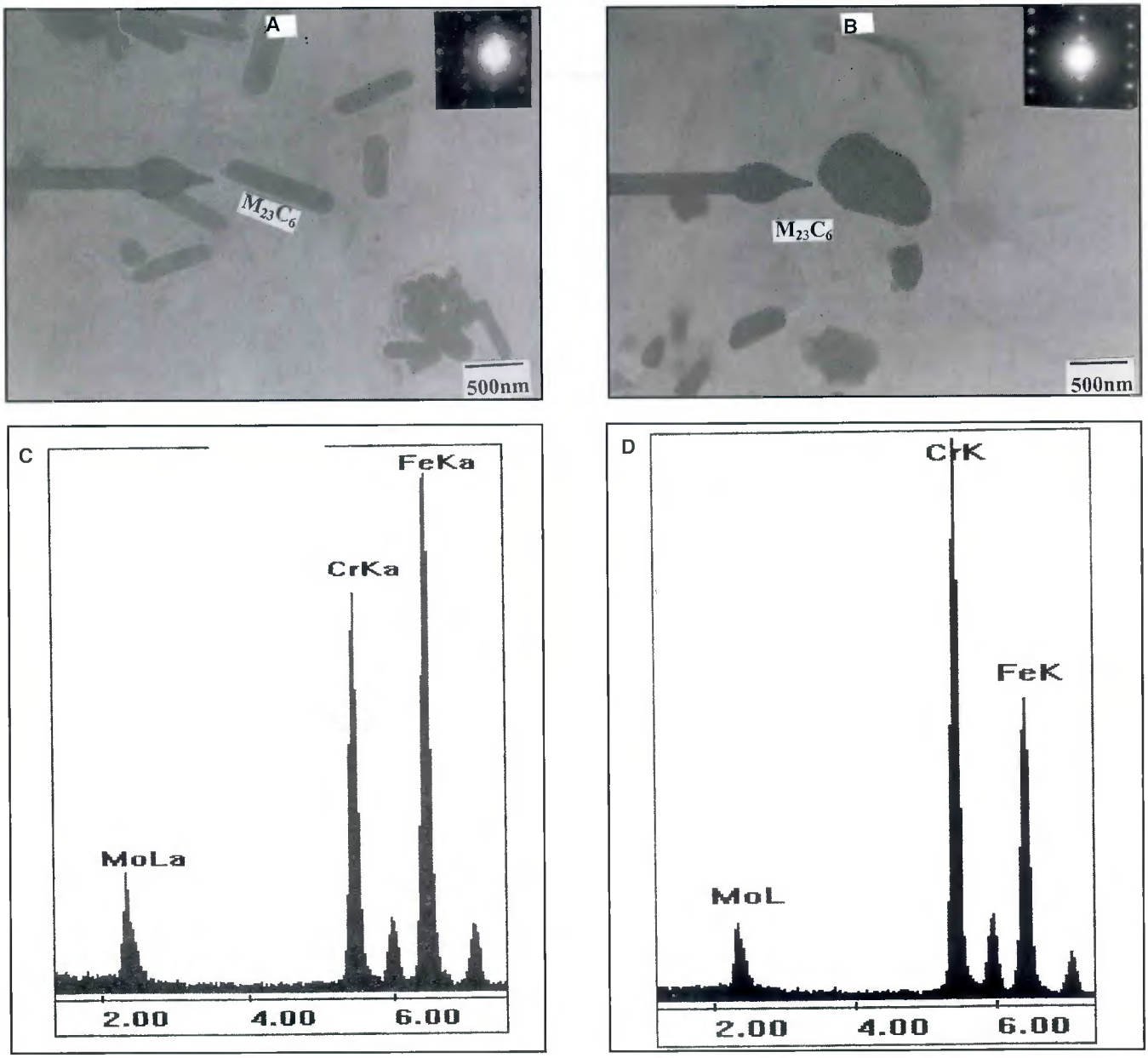

Fig. 4 — TEM micrograph from the hard zone of a weldment after PWHT at 1023 K for 15 h. A — Acicular carbide; B — globular carbide. Insets show SAD patterns from < 2 $\bar{1}$ $\bar{1}$ > of $M_{23}C_6$ (left) and < 3 2 1 > of $M_{23}C_6$ (right); C and D — EDAX spectra showing the presence of Fe-rich and Cr-rich carbides, respectively.

iron or chromium and quantification of the spectra showed that the acicular precipitate had a stoichiometry of $Fe_{11.7}Cr_{7.7}Mo_{3.6}C_6$, while the stoichiometry of globular precipitate was $Fe_{7.1}Cr_{11.2}Mo_{4.7}C_6$. The above observations clearly illustrate that the type of precipitate is $M_{23}C_6$ even though it forms in different morphologies and microchemistry. Similar observations were made for other PWHT times also.

Figure 5A shows the electron micrograph of a region in the hard zone very close to the interface (~20 μm) for PWHT of 15 h. It was found that in addition to the predominantly found $M_{23}C_6$, a bulky cuboidal carbide was also present. Analysis of the SAD pattern inset in Fig. 5A shows that it belongs to the M_6C type. The additional inset in Fig. 5A is the SAD pattern taken along < $\bar{1}$ $\bar{1}$ 1 > of $M_{23}C_6$ having acicular morphology present adjacent to M_6C. The corresponding EDAX spectra for a molybdenum-rich M_6C and Fe-rich $M_{23}C_6$ are given in Fig. 5B and C, respectively. The above results show that $M_{23}C_6$ and M_6C carbides coexist in the hard zone close to the interface.

At short aging times of 1 and 2 h, high density of carbides of the $M_{23}C_6$ type along with very few fine carbides were observed in regions very close to the interface (Fig. 6A), which were found to be molybdenum rich — Fig. 6B. These were identified as Mo-rich M_2C by comparing with the spectra for M_2C available in literature (Ref. 2). As the exposure time was increased to 5 h, it was observed that $M_{23}C_6$ type of carbides were predominant. A typical distribution of carbides for 5 h is shown in Fig. 7A. The inset in Fig. 7A shows the SAD pattern from a representative carbide, which confirms that it belongs to $M_{23}C_6$ along < 1 0 0 >. The corresponding EDAX spectra is given in Fig. 7B. Analysis for all PWHT times show that the $M_{23}C_6$ carbides are either Fe or Cr rich, while the M_6C carbide is rich in Mo. The

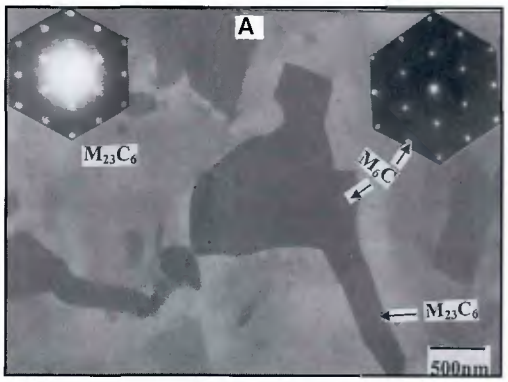

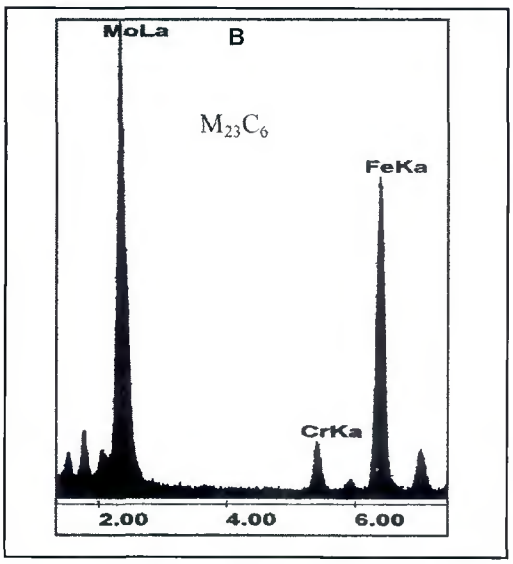

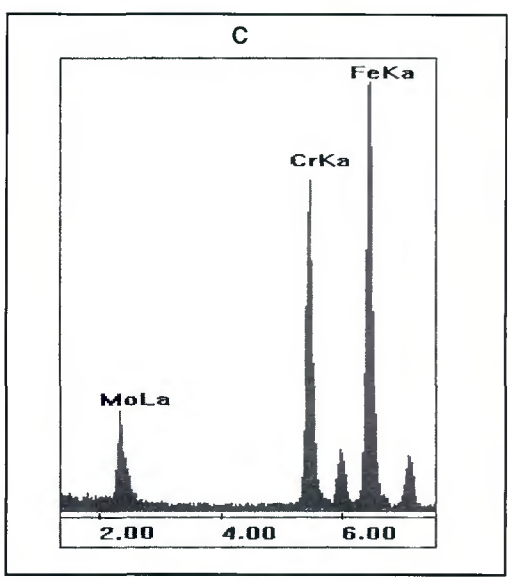

Fig. 5 — A — TEM micrograph showing carbides present in hard zone very close to the interface for PWHT at 1023 K for 15 h. Inset shows SAD pattern obtained along $< \bar{1}\,\bar{1}\,1 >$ $M_{23}C_6$ (left) and $< \bar{1}\,\bar{1}\,1 >$ of M_6C (right); B — EDAX spectra from M_6C molybdenum-rich carbide; C — EDAX spectra from $M_{23}C_6$ carbide showing it to be iron rich.

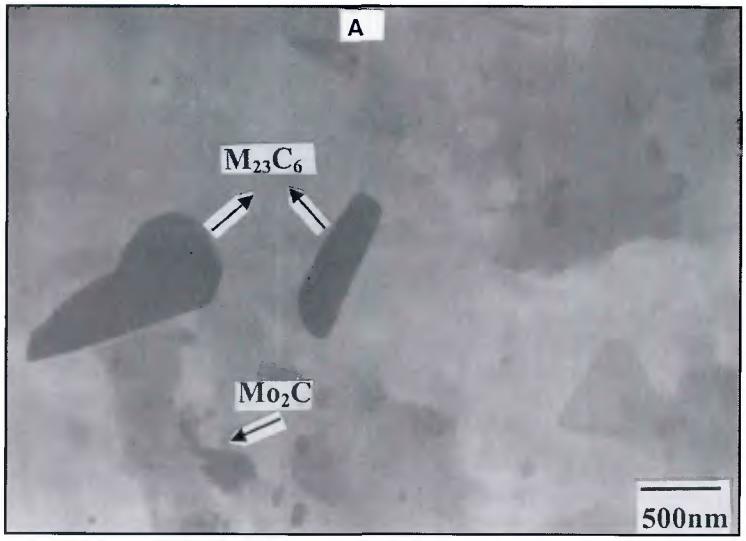

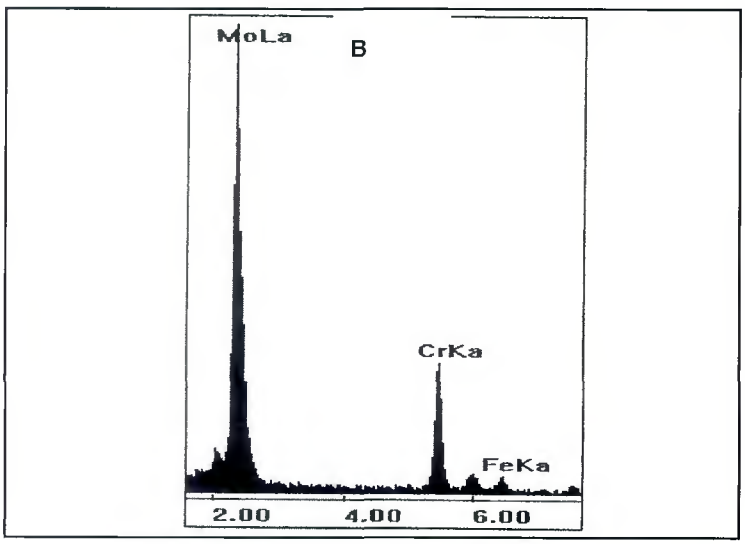

Fig. 6 — Evidence for the presence of Mo_2C in a weldment subjected to PWHT of 1023 K for 1 h. A — TEM micrograph; B — EDAX spectra.

composition of $M_{23}C_6$ carbides was not unique, and both Fe- and Cr-rich $M_{23}C_6$ carbides were observed at all exposure times. There was a steep increase in average Cr/Fe ratio as the PWHT time was increased from 1 to 15 h — Fig. 8. However, there was no appreciable change in the average molybdenum content of carbides. In addition to the Cr/Fe ratio, the size of the precipitates also increased with PWHT time. The above observations show that the three types of carbides, namely $M_{23}C_6$, M_2C, and M_6C, have distinct chemical compositions (Table 3), and microchemistry could be used as a signature to classify the carbides. The details of chemical composition and the stoichiometry of carbides obtained from microchemical analysis are provided in Table 4.

Analysis of regions in the soft zone (region B in Fig. 2B) adjacent to the interface showed it almost devoid of carbides, which also explains its low hardness levels. The TEM micrograph from an isolated carbide in the soft zone after 15 h of exposure is shown in Fig. 9A. The EDAX spectrum in Fig. 9B shows that it is Mo rich, having signatures of M_6C type.

Extensive studies on 9Cr-1Mo steel and 2¼Cr-1Mo carried out in our laboratory (Refs. 11, 12) show that chromium-rich M_2X and $M_{23}C_6$ are the only two types of carbides that form in 9Cr-1Mo steel and molybdenum-rich M_6C and M_2C are the carbides typical of low-Cr steels. The identity of X in M_2X could not be established in our laboratory, although it is reported (Ref. 13) that it is of Cr_2N type. In the present study, although the observation of

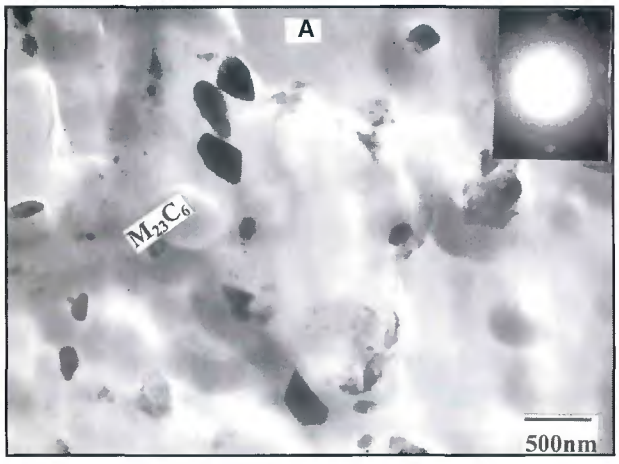

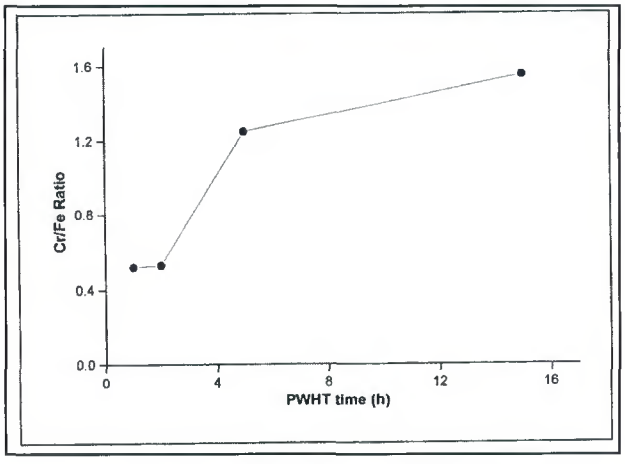

Fig. 8 — Variation of Cr/Fe ratio with PWHT time.

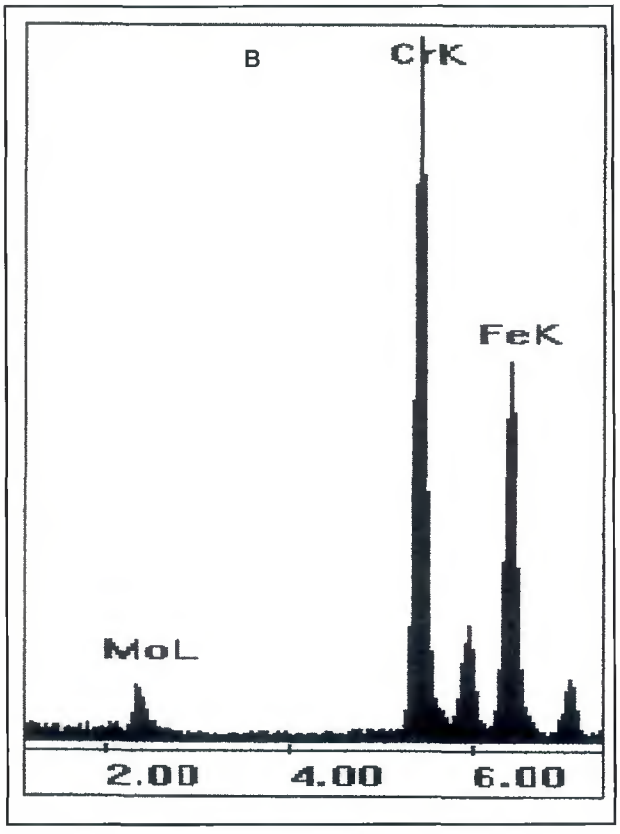

Fig. 7 — Carbides in the hard zone after exposure for 5 h. Inset shows SAD patterns from < 1 0 0 > $M_{23}C_6$. A — Transmission electron micrographs; B — EDAX spectra showing Cr-rich $M_{23}C_6$.

$M_{23}C_6$ in the hard zone of 9Cr-1Mo steel is as expected, no Cr-rich M_2X type of precipitate was observed. Also, the occasional presence of Mo-rich M_2C and M_6C in the hard zone very close to the interface is rather unexpected. This suggests that there could be a redistribution of the substitutional element Cr across the interface as a result of PWHT. Therefore, electron microprobe analysis was carried out to get an elemental redistribution profile of Cr across the interface, which is given in Fig. 10. An EPMA profile shows that there is a redistribution of Cr across the interface, up to a distance of about 10–20 μm.

Having studied the crystallography and microchemistry of carbides in the hard zone, the evaluation of carbon content in different slabs of hard zone (as described in the previous section) requires the input parameters of the chemical compositions of carbides and total area fraction of carbides in each slab.

The chemical compositions of carbides, especially the carbon content, were evaluated using an indirect method given in Appendix 1. The total area fraction of carbides in each slab within the hard zone was measured and plotted in Fig. 11A for a sample aged at 1023 K for 15 h. It was found that A_p is maximum at a distance of 20 μm from the interface, followed by a gradual decrease as the distance from the interface increased. Assuming that α-ferrite is relieved completely of its carbon supersaturation after 15 h of aging at 1023 K, the total amount of carbon in each slab in the hard zone was calculated using the mass balance equation. Figure 11A also shows the variation in carbon concentration and area fraction of carbides with distance across the hard zone. It is clear the carbon profile follows the same trend as that of area fraction of carbides. Figure 11B illustrates the variation of hardness across the complete weldment for PWHT time of 15 h in which it is seen that the hardness is maximum in a narrow region of 100 μm. When this observation is analyzed in conjunction with Fig. 11A, where A_p and C_0 is maximum in the same region, it may be inferred that the high hardness value of the hard zone is indeed due to the carbon
enrichment.

Discussion

It is noted that in the dissimilar weldments of this study, the concentration of carbon in the 2¼Cr base metal side is higher than that of the 9Cr weld metal side (Ref. Table 1). Carbon is observed to diffuse from 2¼Cr-1Mo base metal into 9Cr-1Mo weld metal during PWHT. This can be understood in terms of the role of the alloying additions, mainly substitutional alloy content, which alters the activity of carbon from 0.19 on the low-alloy steel to 0.007 in the 9Cr-1Mo weld metal.

Carbon activity values have been calculated from the following equations, which have been derived using data from 2¼Cr-1Mo and 9Cr-1Mo steels with carbon content varying in the range of 0.009 to 0.12 and 0.068 to 0.12-wt%, respectively.

$$\ln C_{2¼Cr\text{-}1Mo}\ (\text{wt-}\%) = -1.12 + 0.61 \ln a_C \quad \text{(Ref. 14)}$$

$$C_{9Cr\text{-}1Mo}\ (\text{wt-}\%) = 0.16\, a_C^{0.14} + 10.5 a_C^{2.2} \quad \text{(Ref. 15)}$$

where a_C = carbon activity.

Due to the diffusion of carbon during PWHT, microscopic regions across the weldment get enriched in carbon to a higher concentration level than the solubility limit of carbon. The diffusing carbon combines with the substitutional elements present in solution on the high-Cr side and gets precipitated in the form of carbides to form the

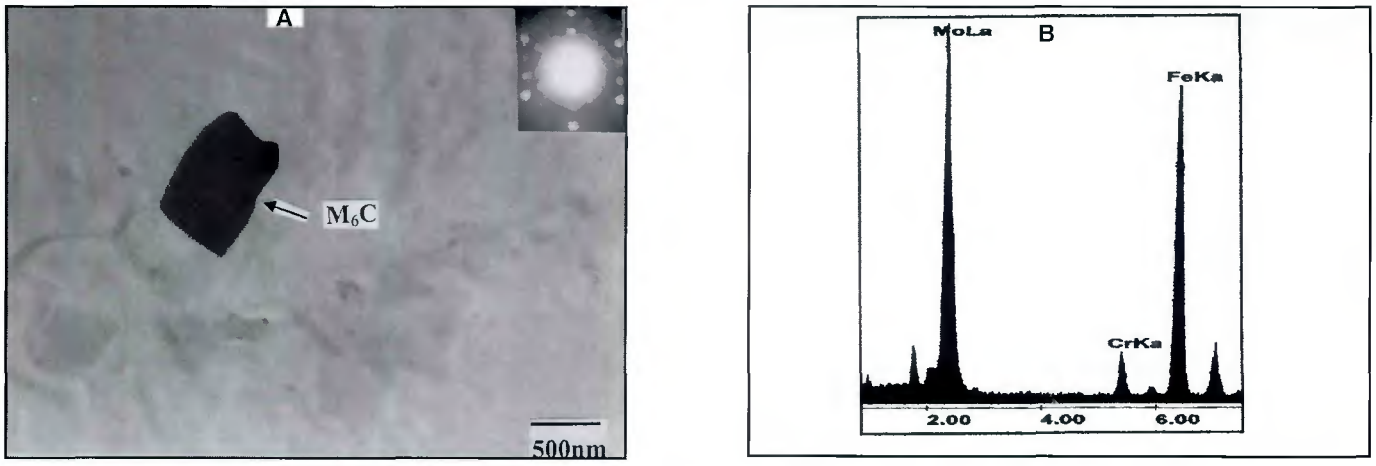

Fig. 9 — TEM micrograph (A) and EDAX spectrum (B) from a M_6C carbide present in the soft zone of the weldment exposed at 1023 K for 15 h.

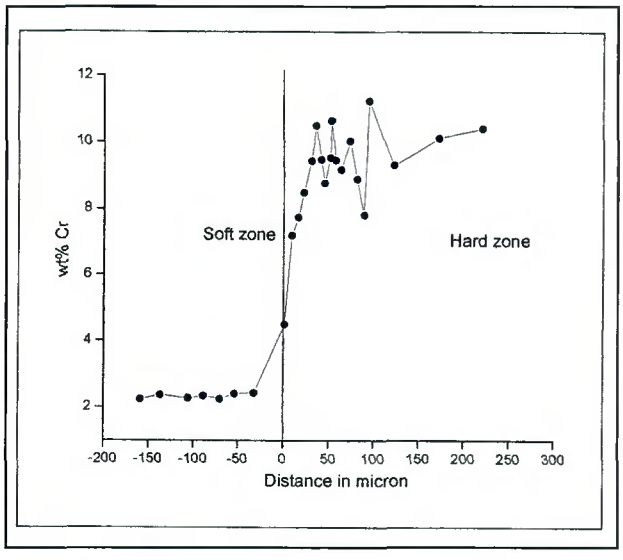

Fig. 10 — EPMA profile showing Cr redistribution across the interface.

hard zone. Since the hard zone (marked A in Fig. 2B) has a high density of fine precipitates, its hardness is found to be higher than other regions of the weldment. Diffusion of carbon due to the presence of an activity gradient across the interface disturbs the thermodynamic equilibrium on the low-Cr side. In order to maintain the equilibrium, the cementite particles in bainite dissolve and the proeutectoid ferrite grains grow, leading to the formation of a soft zone. The soft zone (marked B in Fig. 2B) thus formed is found to have a lower hardness than the rest of the weldment since its carbon content is low and is almost free of carbides. The width and hardness of these zones were found to increase with PWHT time (Ref. 16). The diffusion of carbon from the low-Cr to high-Cr side and dissolution of preexisting precipitates in the low-Cr side continues till the change in width and hardness saturates due to 1) a decrease in the difference in carbon activity between the two sides; 2) depletion in the level of Cr due to the formation of carbides on high-Cr side, which leads to a reduction in the tendency of carbon to diffuse from 2¼Cr to 9Cr side; 3) low C level in solution on the low-Cr side; and 4) the formation of a high density of carbides in the diffusion paths of carbon atoms, inhibiting further diffusion.

The precipitation sequence of carbides in the hard zone formed on the 9Cr-1Mo side of the weldment were derived based on our observation as follows:

$$\alpha' \rightarrow \alpha + M_{23}C_6 \quad (4)$$

It has been reported in literature (Refs. 17, 18) that M_2X and $M_{23}C_6$ are the only two types of carbides that form in 9Cr-1Mo steel. However, in our study, M_2X was not detected in the hard zone. This is possibly due to the high carbon in the hard zone which favors the precipitation of $M_{23}C_6$ as compared to Cr_2N. It is well understood that the precipitation behavior of supersaturated ferrite depends on many factors like initial concentration of substitutional alloying elements, difference in their affinity toward carbon, efficiency of various carbides to scavenge the carbon from the matrix, and difference in the carbon level of ferrite leading to changes in phase stability of local regions. The rare observation (Figs. 6A and 5A) of precipitates like Mo_2C and M_6C in the hard zone on 9Cr-1Mo side is rather unexpected. Mo_2C and M_6C carbides typical of medium Cr steels are normally observed in 2¼Cr-1Mo steel and also observed in high-Cr steels only after prolonged service exposure of 45,000 h (Refs. 11, 19). The EPMA profile in Fig. 10 shows that there is indeed a redistribution of Cr across the interface, up to a distance of about 10–20 μm. Chromium content in the hard zone at the interface is low and increases with distance from the interface. Further, the high carbon content in this region reduces the net chromium equivalent (Cr equivalent of a steel ~ [Cr] + 6[Mo] – 40[C]) (Ref. 20). The observation of Mo-rich carbides together with $M_{23}C_6$ in this region suggests that the steel behaves like a low- or medium-chromium steel. As the Cr content increases, the behavior becomes typical to that of a 9Cr-1Mo steel beyond a distance of 10–20 μm from the interface, although the high carbon prevents the formation of M_2X.

A detailed analysis of the composition values of $M_{23}C_6$ shows significant rearrangement taking place in Fe and Cr values. The ratio of composition of Cr to Fe inside $M_{23}C_6$ was found to increase with aging time from 1 to 15 h — Fig. 8. The Mo content remained more or less the same. This variation in the microchemistry can be understood in terms of the high solubility of Fe and Cr in $M_{23}C_6$. The solubility of Fe in $M_{23}C_6$ has a wide range although the equilibrium $M_{23}C_6$ corresponds to $Cr_{23}C_6$. It is known that (Ref. 18) $Cr_{23}C_6$ is the most stable carbide in 9Cr-1Mo steel in the temperature range of 823–1023 K. At shorter durations, lower mobility of Cr atoms and abundant availability of Fe atoms could have facilitated a higher flux of Fe atoms at the precipitate to matrix interface. This could have resulted in the lower value of Cr/Fe ratio. For longer durations, sustained mobility of Cr atoms and the thermodynamic driving force to approach the chemistry of equilibrium precipitate outweighs the effect of higher availability of Fe atoms around each precipitate, thus resulting in a higher Cr/Fe ratio. Such a variation in

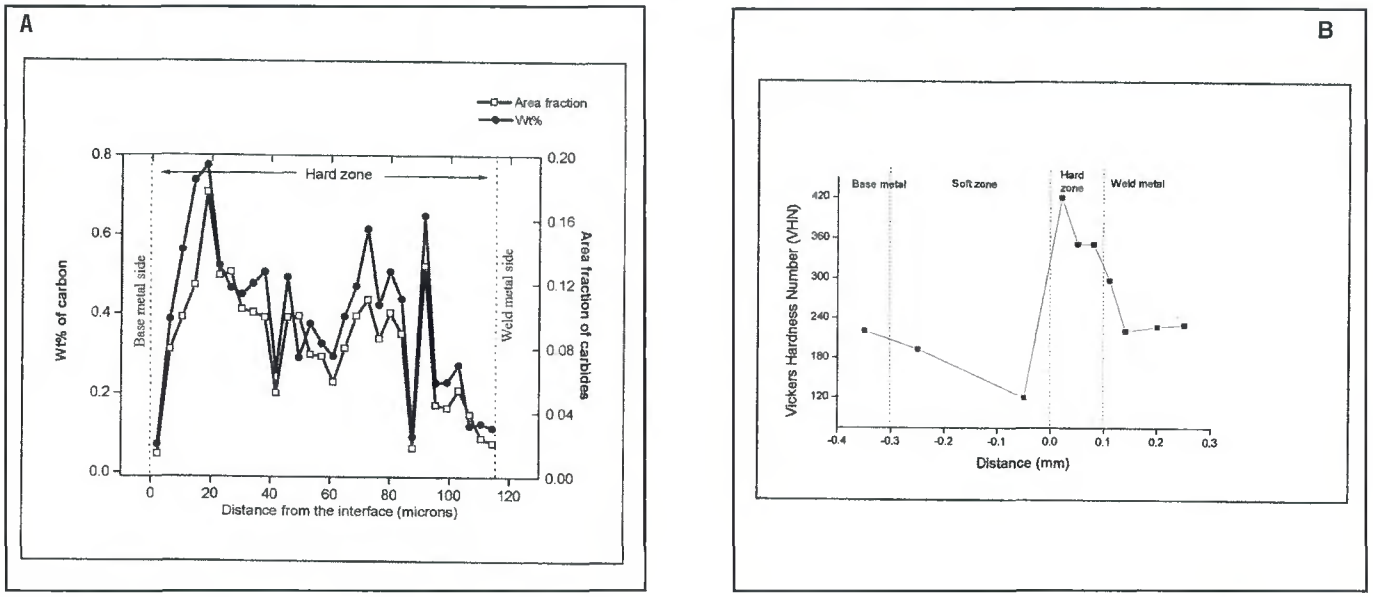

Fig. 11 — A — Variation of carbon concentration and area fraction of carbides across the hard zone after 15 h at 1023 K; B — hardness profile across the weldment after PWHT.

Cr/Fe ratio has been observed in the case of wrought 9Cr-1Mo steel (Ref. 21).

In low-Cr steels, observation of Mo_2C and M_6C can be understood as follows:

The higher affinity of Mo for C offsets Cr-C interaction, favoring the formation of Mo_2C. When the equilibrium gets disturbed on the low-Cr side due to the migration of carbon, these precipitates dissolve leading to an increase in C and Mo concentration in the matrix. Due to availability of more Mo atoms in the matrix, the equilibrium shifts toward M_6C at higher PWHT times, as seen in Fig. 9A in the soft zone of 2¼Cr-1Mo steel. It is known that M_6C is the equilibrium carbide in the proeutectoid ferrite in 2¼Cr-1Mo steel (Ref. 19).

This investigation shows for the first time the variation of carbon content across the weldment of 2¼Cr-1Mo and 9Cr-1Mo after PWHT. Any direct method for the determination of carbon content, such as the chemical method, was not suitable due to the distribution of low amounts of carbon (0.02 to 0.12%) across microscopic regions of the order of a few microns. Hence, an indirect method was adopted to evaluate the concentration of carbon in the hard zone. It is assumed that α-ferrite is relieved completely of its supersaturation after 10 h of aging at 1023 K and its carbon content reaches the solubility limit, which is known. This assumption is valid since the rate of growth of the hard zone was constant after 10 h, as shown in our earlier study (Ref. 16). Hence, carbon content in α-ferrite can be taken as the equilibrium content of carbon in α-ferrite for a weldment subjected to PWHT for 15 h. Using the mass balance equation, the total amount of carbon in each slab in the hard zone was calculated and the variation of carbon concentration across the hard zone was obtained. The average carbon content in the hard zone was found to be 0.39%.

Since the area fraction of precipitates was higher near the interface, the carbon concentration was also high close to the interface, and it is expected to follow the same trend as that of the area fraction, which has also been confirmed. Thus, direct evidence has been provided for enrichment of carbon and precipitation of secondary carbides in the hard zone formed during PWHT of dissimilar weldments.

Conclusions

Based on the above study, the following conclusions may be drawn:

1) Analytical electron microscopy study on carbon extraction replicas taken from the hard zone provided direct evidence for the precipitation of carbides in the hard zone of dissimilar weldments between 9Cr-1Mo and 2¼Cr-1Mo steels subjected to PWHT.

2) The precipitation sequence and microchemistry of secondary phases in hard and soft zones have been established.

3) An indirect method was adopted to calculate the composition of carbides in the hard zone based on the type, amount, and microchemistry. Variation of carbon content across the hard zone was calculated, and it was found to follow the A_p vs. distance profile. Average carbon content in the hard zone was found to be 0.39%.

Acknowledgments

The authors would like to thank Baldev Raj, director, Indira Gandhi Center for Atomic Research, and V. S. Raghunathan, associate director, Materials Characterization Group, for their keen interest and constant support. S. K. Albert, scientific officer, Materials Technology Division, IGCAR, is also acknowledged for his support.

References

1. Albert, S. K., Gill, T. P. S., Tyagi, A. K., Mannan, S. L., Kulkarni, S. D., and Rodriguez, P. 1997. Soft zone formation in dissimilar welds between two Cr-Mo steels. *Welding Journal* 76(3): 135-s to 142-s.

2. Lundin, C. D., Khan, K. K., Yang, D. 1996. Effect of Carbon Migration in Cr-Mo Weldments on Metallurgical Structure and Mechanical Properties. Report No. I. WRC Bulletin 407: 1–49.

3. Lundin, C. D. 1986. Advances in *Welding Science and Technology*. p. 475, ASM International, Materials Park, Ohio.

4. Million, B., Michalicka, P., Pavlovsky, J., and Vrestal, J. 1993. Carbon redistribution in ferritic steel weldments induced by small concentration difference of alloying element. Scripta Materialia. 29: 1039–1041.

5. Lundin, C. D., Khan, K. K., and Yang, D. 1990. Recent trends in welding science and technology. p. 291, ASM International, Materials Park, Ohio.

6. Albert, S. K., Srinivasan, G., and Gill, T. P. S. 1997. Effect of soft zone on tensile properties of a dissimilar weld between two Cr-Mo steels. Proc. *National Welding Seminar*, IIW, pp. 222–232, Bangalore.

7. Buchmayr, B., Cerjak, H., Witwer, M.,

and Kirkaldy, J. S. 1990. Recent trends in welding science and technology. p. 237, ASM International, Materials Park, Ohio.

8. Kim, B. C., Ann, H. S., and Song, J. T. 1992. International trends in welding science and technology. p. 307, ASM International. Materials Park, Ohio.

9. Race, J. M., and Bhadeshia, H. K. D. H. ibid. p. 315.

10. Buchmayer, B. 1993. *Mathematical Modeling in Weld Phenomena*. p. 227, IIM, London.

11. Saroja, S., Parameswaran, P., Vijayalakshmi, M., and Raghunathan, V. S. 1995. Prediction of microstructural states in Cr-Mo steel using phase evolution diagrams. *Acta Metall. Mater* 43(8): 2985–3000.

12. Parameswaran, P., Vijayalakshmi, M., Shankar, P., and Raghunathan, V. S. 1993. Influence of carbon content on microstructure and tempering behavior of 2¼Cr-1Mo steel. J. Mat. Sci. 28(20): 5426–5434.

13. Sanderson, S. J. 1978. Interrelationships between mechanical properties and microstructure in a 9Cr-1Mo steel. Proc. Int. Conf. on Ferritic Steels for Fast Reactor Steam Generators. Ed. S. F. Pugh. and E. A. Little. pp. 120–123, BNES, London.

14. Natesan, K., Chopra, O. K., and Kassener, T. F. 1976. Compatibility of Fe-2.25 wt-% Cr-1wt%Mo steel in a sodium environment. *Nucl. Technol.* 28: 441–451.

15. Chopra, O. K., Natesan, K., and Kassner, T. F. 1981. Carbon and nitrogen transfer in Fe-9Cr-Mo ferritic steels exposed to sodium environment. *J Nucl.Mat.* 96: 269–284.

16. Sudha, C., Terrance, A. L. E., Albert, S. K., and Vijayalakshmi, M. 2002. Systematic study of formation of soft and hard zones in dissimilar weldments of Cr-Mo steels. *J. Nucl. Mat.* 302: 193–205.

17. Senior, B., Noble, F. W., and Eyre, B. L. 1988. The effect of aging on the ductility of 9Cr-1Mo steel. *Acta Metall. Mater.* 36(7): 1855–1862.

18. Saroja, S., Vijayalakshmi, M., and and Raghunathan, V. S. 1992. Influence of cooling rates on the transformation behaviour of 9Cr-1Mo-0.07C steel. *J. Mater. Sci* 27(9): 2389–2396.

19. Jin Yu. 1989. Carbide stability diagrams in 2.25Cr-1Mo steels. *Metallurgical. Transactions.* 20A: 1561–1563

20. Saroja, S., Vijayalakshmi, M., and Raghunathan, V. S. 1992. Influence of solution treatment on the microstructure of 9wt%Cr-1wt%Mo-0.07wt%C steel. *Mat. Sci. Eng.* A154: 59–67.

21. Saroja, S., Vijayalakshmi, M., and Raghunathan, V. S. 1993. Effect of prolonged exposure of 9Cr-1Mo-0.07C steel to elevated temperature. Mater. Trans. JIM 34: 901–906.

Appendix 1

The procedure adopted to arrive at the microchemistry of carbides in the hard zone is discussed in detail as follows:

1. Based on the analysis of SAD pattern, the type of carbide is identified (e.g., $M_{23}C_6$).

2. The X-ray spectra from the carbides are analyzed using the procedure of normalizing the contents of the elements, Fe, Cr, and Mo except carbon. Thin foil approximation was used and absorption correction was applied.

3. The result of the above step does not give the composition of the carbide, but it does give the content of Fe, Cr, and Mo in M in the carbide (e.g., $M_{23}C_6$).

4. Since the formula of the carbide and the specific ratio of the content of the three elements are known, the stoichiometry of the carbide is calculated as follows:

$$X_{Fe} = \frac{\%Fe \text{ in } M}{100} \times 23 \text{ (in this case)} \quad (1A)$$

Value for X_C is taken as 6 in this carbide.

5. Based on the evaluated stoichiometry of the carbide, the wt-% of each element was estimated using the equation

$$Wt\% \text{ of } Fe = \frac{X_{Fe}A_{Fe}}{X_{Fe}A_{Fe} + X_{Cr}A_{Cr} + X_{Mo}A_{Mo} + X_C A_C} \quad (2A)$$

Where A_{Fe}, A_{Cr}, A_{Mo}, and A_C refer to the atomic weight of Fe, Cr, Mo, and C, respectively. The statistical error for 99% confidence limit ($\pm 2\sigma$) in the calculation of around ten spectra is about ± 2% for Fe, ± 4% for Cr, and ± 6% for Mo.

6. Using the above method, the carbon content in each type of precipitate was evaluated.

Preparation of Manuscripts for Submission to the *Welding Journal* Research Supplement

All authors should address themselves to the following questions when writing papers for submission to the Welding Research Supplement:

- Why was the work done?
- What was done?
- What was found?
- What is the significance of your results?
- What are your most important conclusions?

With those questions in mind, most authors can logically organize their material along the following lines, using suitable headings and subheadings to divide the paper.

1) **Abstract.** A concise summary of the major elements of the presentation, not exceeding 200 words, to help the reader decide if the information is for him or her.

2) **Introduction.** A short statement giving relevant background, purpose, and scope to help orient the reader. Do not duplicate the abstract.

3) **Experimental Procedure, Materials, Equipment.**

4) **Results, Discussion.** The facts or data obtained and their evaluation.

5) **Conclusion.** An evaluation and interpretation of your results. Most often, this is what the readers remember.

6) **Acknowledgment, References and Appendix.**

Keep in mind that proper use of terms, abbreviations, and symbols are important considerations in processing a manuscript for publication. For welding terminology, the *Welding Journal* adheres to AWS A3.0:2001, *Standard Welding Terms and Definitions.*

Papers submitted for consideration in the Welding Research Supplement are required to undergo Peer Review before acceptance for publication. Submit an original and one copy (double-spaced, with 1-in. margins on 8 ½ x 11-in. or A4 paper) of the manuscript. A manuscript submission form should accompany the manuscript.

Tables and figures should be separate from the manuscript copy and only high-quality figures will be published. Figures should be original line art or glossy photos. Special instructions are required if figures are submitted by electronic means. To receive complete instructions and the manuscript submission form, please contact the Peer Review Coordinator, Doreen Kubish, at (305) 443-9353, ext. 275; FAX 305-443-7404; or write to the American Welding Society, 550 NW LeJeune Rd., Miami, FL 33126.